ACS Biomaterials SCIENCE & ENGINEERING

Article

pubs.acs.org/journal/abseba

Controlled Tubular Unit Formation from Collagen Film for Modular Tissue Engineering

Jianming Sang,[†] Xiang Li,[†] Yue Shao,[†] Zida Li,[†] and Jianping Fu[*,†,‡,§,∥]

[†]Department of Mechanical Engineering, University of Michigan, 2350 Hayward Street, Ann Arbor, Michigan 48109, United States

[‡]Michigan Center for Integrative Research in Critical Care, University of Michigan, 2800 Plymouth Road, Ann Arbor, Michigan 48109, United States

[§]Department of Biomedical Engineering, University of Michigan, 2200 Bonisteel Boulevard, Ann Arbor, Michigan 48109, United States

[∥]Department of Cell and Developmental Biology, University of Michigan, 109 Zina Pitcher Place, Ann Arbor, Michigan 48109, United States

Supporting Information

ABSTRACT: Bottom-up or modular tissue engineering is one of the emerging approaches to prepare biomimetic constructs *in vitro*, involving fabrication of small tissue units as building blocks before assembling them into functional tissue constructs. Herein, we reported a microscale tissue engineering approach to generate tubular tissue units through cellular contractile force induced self-folding of cell-laden collagen films in a controllable manner. Self-folding of cell-laden collagen films was driven by film contraction resulted from intrinsic contractile property of adherent mammalian cells seeded in collagen films. We explored in detail independent effects of collagen gel concentration, cell density, and intrinsic cellular contractility on self-folding and tubular structure formation of cell-laden collagen films. Through both experiments and theoretical modeling, we further demonstrated the effectiveness of integrating ridge array structures onto the backside of collagen films in introducing structural anisotropy and thus controlling self-folding directions of collagen films. Our approach of using ridge array structures to introduce mechanical anisotropy and thus promote tubular tissue unit formation can be extended to other biomaterial systems and thus provide a simple yet effective way to prepare tubular tissue units for modular tissue engineering applications.

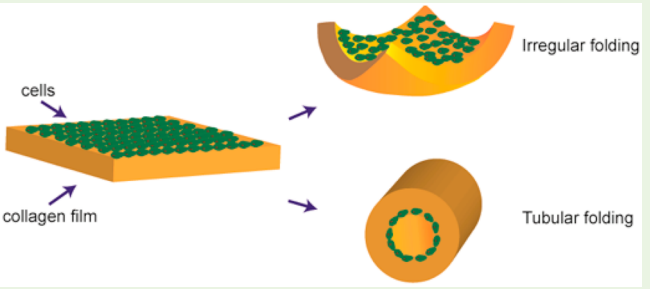

KEYWORDS: *tubular structure, cellular contractile force, bottom-up tissue engineering*

INTRODUCTION

Tissue engineering develops various three-dimensional (3D) biological constructs with the aim of restoring and improving the functionality of damaged tissues and organs caused by diseases or aging.[1,2] Tubular structure, for example, exists in multiple forms *in vivo* such as blood vessels, lymph vessels, trachea, and intestines and plays a vital role in maintaining the homeostasis of our body. *In vitro* construction of tubular structures that mimic tissue-specific spatial cellular distribution and intricate microstructures is of utmost importance for fulfilling the promise of tissue engineering to restore the functionality of damaged tubular tissues and organs. Traditional tissue engineering methods employ a top-down approach to prepare *in vitro* constructs, in which cells are loaded into a biodegradable scaffold, where they populate, secrete extracellular matrix (ECM), remodel tissue microarchitecture, and finally generate 3D functional biological constructs.[3−8] However, it is still challenging for top-down approaches to develop tissue constructs that can recapitulate intricate microstructural features of *in vivo* tissues with proper tissue-specific spatial cellular distributions. Furthermore, mass transfer limitation remains a significant hurdle for tissue engineering to develop large, complex, and functional tissue constructs.[9]

Over the past decade, bottom-up or modular tissue engineering has emerged as an alternative, promising approach for functional tissue engineering.[10,11] In modular tissue engineering, small tissue units are first prepared as building blocks before being assembled into functional, large-scale constructs. Such small tissue units can be prepared using various techniques such as self-assembled cellular aggregation,[12] microfabrication of cell-laden hydrogels,[13] and cell sheet technology.[14] For instance, Torres-Rendon et al. have reported an approach to generate free-standing tubular constructs using cellulose nanofibril hydrogel tubes as sacrificial templates.[15]

Special Issue: Multiscale Biological Materials and Systems: Integration of Experiment, Modeling, and Theory

Received: August 10, 2016
Accepted: October 10, 2016

DOI: 10.1021/acsbiomaterials.6b00468
ACS Biomater. Sci. Eng. XXXX, XXX, XXX−XXX

Baek et al. have developed a self-folding-based approach to generate a multiwalled gel tube by constructing a gel patch consisting of two layers with significantly different stiffness and capacities for uptaking water.[16] More recently, L'Heureux et al. have reported a cell sheet technology to construct tissue-engineered blood vessels (TEBVs) suitable for autologous small-diameter arterial revascularization in adults.[17] Compared with top-down approaches, bottom-up methods afford more engineering control over spatial cellular distribution and tissue organization, thus offering the advantage of recapitulating microarchitecture of native tissues and creating biomimetic engineering constructs.[11]

In this study, we reported a microscale tissue engineering approach to generate tubular tissue units through cellular contractile force induced self-folding of cell-laden collagen films in a controllable manner. Self-folding of cell-laden collagen films was driven by film contraction resulted from an intrinsic contractile property of adherent mammalian cells seeded in collagen films. Collagen, as a major component of fibrillar ECM *in vivo*, has been widely used in tissue engineering as supporting biomaterials.[18−22] Cellular contraction-induced folding of collagen matrices occurs in a variety of *in vivo* situations such as embryonic development[23] and wound healing.[24] In recent years, different cell-laden microscale tissue constructs have been developed using cellular contractile forces as driving forces to control tissue construct folding and shapes.[25−27] However, these previous studies have not yet explored in detail different experimental parameters involved in cell-laden collagen films and their independent effects on collagen film self-folding. Furthermore, precise engineering control of self-folding directions of collage tubular structures have not yet been reported. Herein, we explored in detail independent effects of collagen gel concentration, cell density, and intrinsic cellular contractility on self-folding and tubular structure formation of cell-laden collagen films. Using carefully designed experiments and detailed simulations and theoretical studies, we further demonstrated the effectiveness of integrating ridge array structures onto the backside of collagen films in introducing structural anisotropy and thus controlling self-folding directions of collage films. The approach demonstrated in this work using ridge array structures to introduce mechanical anisotropy and thus promote tubular tissue unit formation from cell-laden collagen films can be easily extended to other biocompatible material systems and thus provide a simple yet effective way to prepare tubular tissue units for modular tissue engineering applications.

MATERIALS AND METHODS

Cell Culture. Three different cell types were used in the present study. GFP expressing-endothelial cells (TeloHAEC-GFP, ATCC) is a clonal cell line stably expressing EmGFP under EF1α promoter. TeloHAEC-GFP cells were cultured in vascular cell basal medium (ATCC), supplemented with vascular endothelial cell growth kit-VEGF (ATCC). Human umbilical vein endothelial cells (HUVECs) obtained from Lonza were cultured in fully supplemented endothelial growth medium (EGM-2, Lonza). Human normal lung fibroblasts (MRC-5) from ATCC were cultured in Eagle's Minimum Essential Medium (EMEM) supplemented with 10% fetal bovine serum (FBS, Life Technologies). All cells were maintained in monolayer culture at 37 °C and 5% CO_2. Culture medium was exchanged every other day, and cells were passaged when reaching about 80% confluency.

Microfabrication To Generate Molds. Si molds without ridge structures were fabricated using standard photolithography. Briefly, Si wafers were spin-coated with photoresist SPR 220 followed by UV patterning and deep reactive ion etching (DRIE). Mold thickness was controlled by varying etching time during DRIE.

To generate Si molds with ridge structures, a 2 μm silicon dioxide layer was first generated on top of the Si wafer using thermal oxidation. After photolithography, reactive ion etching (RIE) was performed to pattern the silicon dioxide layer. After stripping photoresist, a new photoresist layer was coated on the Si wafer before photolithography. DRIE was then performed on the wafer to generate chamber structures. After stripping photoresist, another DRIE operation was conducted on the wafer during which the silicon dioxide layer served as etching mask. Finally, the silicon dioxide layer was stripped using hydrogen peroxide solution. The Si wafer was silanized with trichloro(1*H*,1*H*,2*H*,2*H*-perfluorooctyl)silane (Sigma-Aldrich) for 4 h under vacuum to facilitate subsequent release of PDMS molds.

Negative PDMS molds were generated by replica molding. Briefly, PDMS prepolymer (10:1 base-to-curing-agent ratio) was poured over Si molds, cured at 60 °C for 20 h, peeled off from Si molds, and cut into desired dimensions. Before being loaded with cell-laden collagen gel solutions, PDMS molds were first sterilized using 100% ethanol before being treated with air plasma for 30 s followed by incubation in PLL(20)-g(3.5)-PEG(5) solution (SuSoS) for >1 h to aid subsequent release of collagen films.

Collagen Film Preparation. Collagen gel solution was prepared following the vendor's protocol. Briefly, 10× PBS buffer solution (Thermo Fisher Scientific), 1 N sodium hydroxide (Sigma-Aldrich), and purified water were mixed at 4 °C, followed by adding rat-tail collagen type I (Corning) into the mixture to obtain desired final collagen concentration. To prepare cell-laden collagen gel solution, cells were harvested from cell culture using 0.25% Trypsin-EDTA and counted. Cells were collected using centrifugation before being resuspended in collagen gel solutions. Final cell density was controlled by a prescribed loading volume of collagen gel solution.

To generate collagen films, cell-laden collagen gel solution was manually loaded into PDMS molds. Loading volume was precisely controlled on the basis of the size of PDMS molds to ensure constant collagen film thickness. After being loaded with cell-laden collagen solution, PDMS molds were stored at 37 °C for 30 min for gelation of collagen gel solution. Cells would gradually sediment to the bottom of collagen films due to gravity during the gelation process.

For PDMS molds with ridge array structures, PDMS molds were flipped upside down during the gelation process of collagen films to ensure that ridge structures and cells would locate on opposite sides of collagen films. After gelation, collagen films were released from PDMS molds by gently pipetting culture medium. Cell-laden collagen films were maintained in culture medium, which was exchanged every other day. To examine the effect of cellular contractile forces on collagen film folding, 10 μM blebbistatin was supplemented to culture medium maintaining cell-laden collagen films.

Collagen Film Self-Folding. After being released from PDMS molds, free-standing collagen films in culture medium would gradually deform (due to cellular contractile forces) and fold into either irregular structures or regular tubular structures at day 3. In the present study, two parameters were defined and quantified to describe collagen film folding: folded structure ratio defined as the ratio of the number of folded films (either irregular or tubular) to the total number of collagen films and tubular structure ratio defined as the ratio of the number of tubule-forming films to the number of folded collagen films.

The total number of collagen films was counted at day 0, and the numbers of irregular and tubular structures resulted from collagen film self-folding were counted at day 1, day 2, and day 3. Each experiment was repeated three times, and statistical analysis was performed using the OriginLab software.

Cell Viability. Viability of HUVECs in collagen films was assessed at day 0, day 3, and day 7 using the Live/Dead stain kit (Life Technologies). Following the vendor's protocol, cell-laden collagen structures were collected from culture and washed three times with PBS. Collagen structures were incubated in 4.0 μM calcein-AM and 4.0 μM ethidium homodimer-1 dissolved in PBS for 40 min at 37 °C before being washed three times in PBS and imaged using a laser scanning confocal microscope (Nikon Instruments). For each collagen

DOI: 10.1021/acsbiomaterials.6b00468
ACS Biomater. Sci. Eng. XXXX, XXX, XXX−XXX

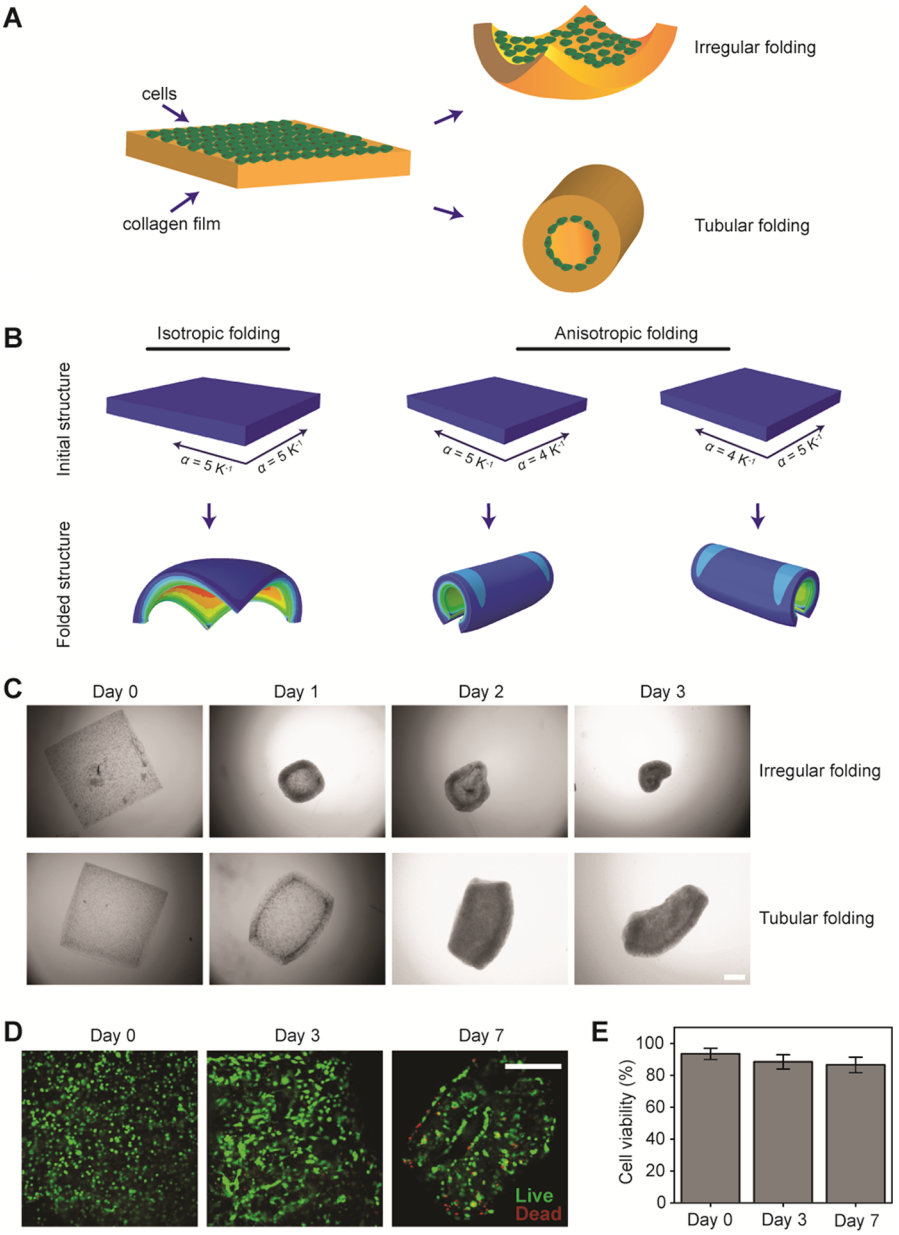

Figure 1. Folding of collagen films into tubular structures using cellular contractile force. (A) Schematic showing collagen film folding owing to cellular contractile force. Square-shaped collagen films with a size of 2 mm × 2 mm that were initially flat folded into either irregular (top) or regular (bottom) tubular structures owing to cellular contractile forces from adherent mammalian cells seeded on one side of the collagen films. (B) Numerical simulation of collagen film folding resulted from either isotropic (left) or anisotropic (right) thermal expansion coefficients of collagen films. In simulations, collagen films were modeled as two-layered, square-shaped structures. The bottom layer had a thickness of 50 μm and either isotropic (left) or anisotropic (right) thermal expansion coefficients as indicated. The top layer had a thickness of 150 μm and a homogeneous thermal expansion coefficient of 0 K^{-1}. Both top and bottom layers had a Young's modulus of 20 KPa. In simulations, film temperature was set to decrease from −273.15 K (0 °C) to −293.15 K (−20 °C). (C) Representative bright field images showing dynamics folding of collagen films into either irregular (top) or tubular (bottom) structures in 3 d. Square-shaped collagen films with a size of 2 mm × 2 mm and a collagen concentration of 4 mg mL^{-1} were initially seeded with TeloHAEC-GFP cells with a cell density of 2 × 10^6 cells mL^{-1}. Scale bar, 500 μm. (D) Representative fluorescence microscopy images showing live (stained green) and dead (stained red) TeloHAEC-GFP cells in 4 mg mL^{-1} collagen films at day 0, day 3, and day 7, as indicated. TeloHAEC-GFP cells were seeded into collagen films with an initial cell density of 2 × 10^6 cells mL^{-1}. Scale bar, 500 μm. (E) Bar plot showing cell viability as a function of culture time. Data represents the mean ± s.e.m. with n = 3.

structure, at least four images were captured, and cell viability was quantified by comparing the number of green-stained cells (live) to the number of red-stained nuclei (dead).

Finite Element Simulation. The commercial finite element package ABAQUS (SIMULIA, Dassault Systèmes) was used for numerical simulations of self-folding of collagen films with different geometries and ridge structures. Self-folding of collagen films due to cellular contractile forces was modeled using thermal contraction.[28] Specifically, collagen films without ridge structures were modeled as two-layered structures. The bottom layer had a thickness of 50 μm and either isotropic or anisotropic thermal expansion coefficients. For isotropic thermal expansion, the bottom layer had an isotropic thermal expansion coefficient of 5 K^{-1}. For anisotropic thermal expansion, the bottom layer had thermal expansion coefficients of 4 and 5 K^{-1} along two orthogonal axes. The top layer had a thickness of 150 μm and a homogeneous thermal expansion coefficient of 0 K^{-1}. For collagen

DOI: 10.1021/acsbiomaterials.6b00468
ACS Biomater. Sci. Eng. XXXX, XXX, XXX−XXX

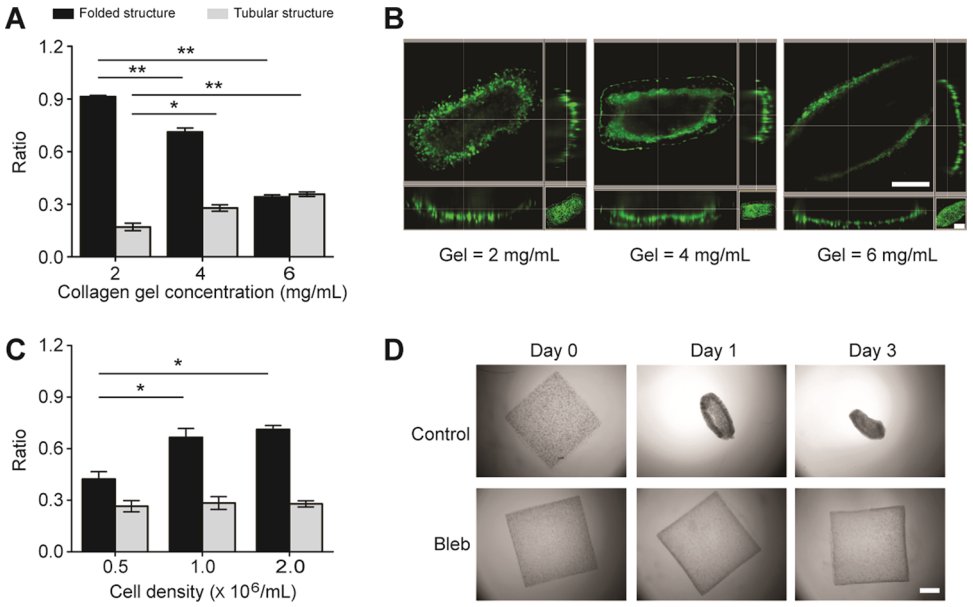

Figure 2. Effects of collagen gel concentration and cell density on collagen film folding. (A) Independent effect of collagen gel concentration on collagen film folding at day 3. Square-shaped collagen films with a size of 2 mm × 2 mm were initially seeded with TeloHAEC-GFP cells with a cell density of 2×10^6 cells mL^{-1}. Collagen concentration was varied from 2 to 6 mg mL^{-1} as indicated. (B) Confocal images showing spatial distributions of TeloHAEC-GFP cells within collagen films with different collagen gel concentrations as indicated at day 3. Scale bar, 500 μm. (C) Independent effect of initial cell seeding density on collagen film folding. Square-shaped collagen films with a size of 2 mm × 2 mm and a collagen concentration of 4 mg mL^{-1} were initially seeded with TeloHAEC-GFP cells with a cell density from 0.5×10^6 to 2×10^6 cells mL^{-1} as indicated. (D) Representative bright field images showing the effect of blebbistatin treatment on collagen film folding. After blebbistatin treatments, most collagen films remained flat at day 3. Square-shaped collagen films with a size of 2 mm × 2 mm and a collagen concentration of 4 mg mL^{-1} were initially seeded with TeloHAEC-GFP cells with a cell density of 2×10^6 cells mL^{-1}. Scale bar, 500 μm. *P* values in (A) and (C) were calculated using two-side unpaired student *t*-tests. *, $p < 0.05$; **, $p < 0.01$. Error bars, s.e.m. with $n = 3$.

films with ridge arrays, collagen films were modeled as three-layered structures. The bottom layer had a thickness of 50 μm and an isotropic thermal expansion coefficient of 5 K^{-1}. The middle layer and the top ridge array had a thickness of 100 and 50 μm, respectively, and both layers had a homogeneous thermal expansion coefficient of 0 K^{-1}. All structural layers had a Young's modulus of 20 KPa and were discretized into tetrahedral mesh elements. In simulations, film temperature was set to decrease from −273.15 K (0 °C) to −293.15 K (−20 °C).

The theoretical moment of inertia (MI) of collagen films (with or without ridge structures) were also calculated to determine relative bending stiffness of collagen films along different axes as

$$\mathrm{MI}_{\mathrm{ridge}} = \frac{1}{12}LT^3 - \frac{1}{3}LH^3 - \frac{1}{8}LHT^2 + \frac{1}{4}LTH^2 \quad (1)$$

and

$$\mathrm{MI}_{\mathrm{non\text{-}ridge}} = \frac{1}{12}L(T-H)^3 \quad (2)$$

where $\mathrm{MI}_{\mathrm{ridge}}$ and $\mathrm{MI}_{\mathrm{nonridge}}$ were the moment of inertia for collagen films along ridges and perpendicular to ridge arrays, respectively, L was the total length of collagen films, T was the film thickness, and H was the ridge height.

RESULTS AND DISCUSSION

Self-Folding of Flat Collagen Films without Ridge Structures. Square-shaped, free-standing flat collagen films with a dimension of 2 mm × 2 mm were first generated using PDMS molds (Supporting Figure 1). Thickness of collagen films was about 200 μm. For cell visualization, a clonal endothelial cell line (TeloHAEC-GFP) stably expressing EmGFP under EF1α promoter was admixed with collagen solutions before gelation to obtain an effective cell density of 2 × 10^6 cells mL^{-1}. As expected, during gelation of collagen films, cells in collagen solutions sedimented to the film bottom due to gravity, forming a uniform cell monolayer within collagen films (Supporting Figure 2). During culture over the following 3 days, free-standing collagen films gradually deformed in culture medium and formed folded structures, most of which were irregularly folded (Figure 1A–C).

We conducted numerical simulations to model self-folding of cell-laden collagen films due to cellular contractile forces as thermal contraction.[28] Simulation results demonstrated that square-shaped collagen films with an isotropic thermal expansion coefficient, in principle, would not fold into regular tubular structures (see Materials and Methods for details; Figure 1B), consistent with dominant irregularly folded collagen film structures observed in experiments for square-shaped collagen films without ridge structures. A few regular tubular structures appeared in experiments at day 3, likely owing to some local nonuniformity of collagen films or cell distribution at the collagen film bottom. Such local nonuniformity effect could also be recapitulated in simulations of self-folding collagen films with anisotropic thermal expansion coefficients. In simulations, square-shaped flat collagen films folded into regular tubular structures along a direction with a greater thermal expansion coefficient and thus larger contraction to facilitate collagen film folding (Figure 1B). Importantly, this numerical calculation suggested a viable approach to control folding directions of flat, cell-laden collagen films and generate regular tubular structures by rendering mechanical anisotropy in collagen films.

To examine cell viability in self-folding collagen films, TeloHAEC-GFP cells were seeded into 4 mg mL^{-1} collagen films with an initial cell density of 2×10^6 cells mL^{-1}. Viability

DOI: 10.1021/acsbiomaterials.6b00468
ACS Biomater. Sci. Eng. XXXX, XXX, XXX−XXX

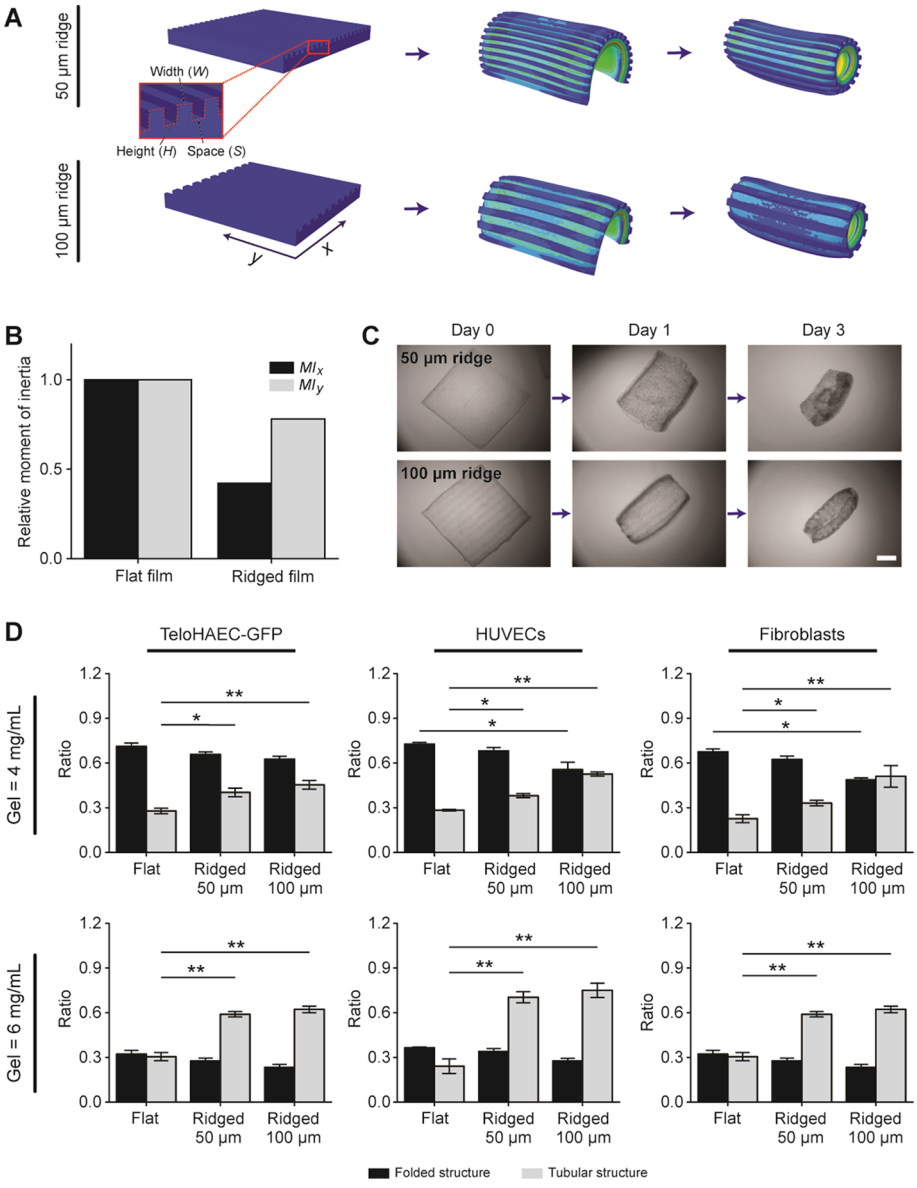

Figure 3. Ridge array structure integrated onto square-shaped collagen films to facilitate collagen film folding. (A) Simulations showing folding of square-shaped collagen films with a size of 2 mm × 2 mm integrated with 50 μm (top) or 100 μm (bottom) ridge array structures, where x-direction was designated as perpendicular to the ridge array and y-direction along ridges. In simulations, collagen films were modeled as three-layered, square-shaped structures. The bottom layer had a thickness of 50 μm and an isotropic thermal expansion coefficient of 5 K^{-1}. The middle layer and the top ridge array had a thickness of 100 and 50 μm, respectively, and both layers had a homogeneous thermal expansion coefficient of 0 K^{-1}. For 50 and 100 μm ridge arrays, ridge width and space were both 50 and 100 μm, respectively. All three layers in the collagen film had a Young's modulus of 20 KPa. In simulations, film temperature was set to decrease from −273.15 K (0 °C) to −293.15 K (−20 °C). (B) Normalized theoretical moment of inertia (MI) for collagen films with or without ridge array structures along x- and y-directions as indicated. Data was normalized to values for flat collagen films without ridges. Please note that the moment of inertial values for collagen films with 50 and 100 μm ridge arrays were the same. (C) Representative bright field images showing folding dynamics of collagen films with 50 μm (top) and 100 μm (bottom) ridge array structures. Square-shaped collagen films with a size of 2 mm × 2 mm and a collagen concentration of 4 mg mL^{-1} were initially seeded with TeloHAEC-GFP cells with a cell density of 2 × 10^6 cells mL^{-1}. Scale bar, 500 μm. (D) Bar plots showing the effect of ridge structures on collagen film folding. Quantitative data from different gel concentrations and cell types were listed. Cell density was kept constant at 2 × 10^6 cells mL^{-1}. P values were calculated using two-side unpaired student t-tests. *, $p < 0.05$; **, $p < 0.01$. Error bars, s.e.m. with $n = 3$.

of TeloHAEC-GFP cells, defined as the ratio of calcein-AM-stained living cells to the total cell count, was 93 ± 4% and uniform throughout the entire collagen film at day 0 (Figure 1D,E). Viabilities of TeloHAEC-GFP cells at day 3 and day 7 were 88 ± 4% and 87 ± 5%, respectively (Figure 1D,E). These results were consistent with previously reported cell viability in 3D hydrogels.[29] Thus, cell viability within self-folding collagen films remained high over at least 1 week in culture medium.

Cellular Contraction Drives Self-Folding of Collagen Films. Self-folding of cell-laden collagen films was driven by film contraction resulted from intrinsic contractile property of adherent mammalian cells seeded in collagen films. Here, we explored in detail independent effects of collagen gel concentration, cell density, and intrinsic cellular contractility on self-folding and tubular structure formation of cell-laden collagen films.

DOI: 10.1021/acsbiomaterials.6b00468
ACS Biomater. Sci. Eng. XXXX, XXX, XXX−XXX

We first examined how collagen gel concentration would affect self-folding of cell-laden collagen films. Square-shaped collagen films with a dimension of 2 mm × 2 mm were initially seeded with TeloHAEC-GFP cells with a cell density of 2×10^6 cells mL^{-1}. When collagen gel concentration was increased from 2 to 6 mg mL^{-1}, folded structure ratio of collagen films, defined as the ratio of the number of folded films (either irregular or tubular) to the total number of collagen films, decreased from 0.91 ± 0.007 to 0.34 ± 0.012 at day 3 (Figure 2A). In contrast, tubular structure ratio, defined as the ratio of the number of tubule-forming films to the number of folded collagen films, increased from 0.17 ± 0.02 to 0.36 ± 0.012 (Figure 2A). A decrease in folded structure ratio with increasing collagen gel concentration was understandable, as a greater bending rigidity of collagen films at a higher collagen gel concentration would make it more difficult for collagen films to deform under the same cellular contraction force. An increase of tubular structure ratio with increasing collagen gel concentration suggested that less flexible collagen films at high collagen gel concentrations might suppress to a certain degree random folding of flat collagen films, resulting in an effective increase in the tubular structure ratio.

Collagen gel concentration can directly impact collagen fibril density, fibril diameter, and mesh size within collagen gels, which can further affect cell migration and redistribution within collagen gels during long-term cell culture.[30] Cells tend to migrate more within collagen gels of lower gel concentrations but migrate less in collagen gels of higher gel concentrations. Before self-folding of cell-laden collagen films, cells within collagen films were distributed as a monolayer. During the 3 day period in collagen films with a gel concentration of 2 mg mL^{-1}, most TeloHAEC-GFP cells migrated away from the initial monolayer location and penetrated deeply into collagen films (Figure 2B). In contrast, for collagen films with a gel concentration of 6 mg mL^{-1}, few TeloHAEC-GFP cells showed significant migration over the 3 day period, and most TeloHAEC-GFP cells appeared to remain in the monolayer (Figure 2B).

We further investigated how cell seeding density would affect self-folding of cell-laden collagen films. Square-shaped collagen films with a dimension of 2 mm × 2 mm and a collagen concentration of 4 mg mL^{-1} were initially seeded with TeloHAEC-GFP cells of a cell density from 0.2×10^6 to 2×10^6 cells mL^{-1}. Intuitively, self-folding of cell-laden collagen films driven by intrinsic cellular contractility should be promoted by increasing cell seeding density, which was consistent with experimental results, where folded structure ratio increased with cell seeding density (Figure 2C). Specifically, very few collagen films folded at day 3 with a cell seeding density $\leq 0.2 \times 10^6$ cells mL^{-1} (data not shown). Folded structure ratio at day 3 increased from 0.42 ± 0.043 to 0.71 ± 0.039 when cell seeding density increased from 0.5×10^6 to 2×10^6 cells mL^{-1} (Figure 2C). Since changes in cell density affected film contraction isotropically, there was no significant effect of increasing cell seeding density on improving the tubular structure ratio at day 3 (Figure 2C).

To specifically examine the importance of intrinsic cellular contractile force for self-folding of collagen films, 10 μM blebbistatin (a specific inhibitor of myosin II) was supplemented to culture medium for square-shaped, cell-laden collagen films (2 mm × 2 mm) with a collagen gel concentration of 4 mg mL^{-1} and seeded with TeloHAEC-GFP cells at a cell density of 2×10^6 cells mL^{-1}. Blebbistatin treatment effectively blocked cellular contractile force and thus completely inhibited self-folding of cell-laden collagen films by day 3 (Figure 2D).

Controlled Collagen Film Folding via Ridge Structures. Intrinsic irregular, random self-folding of squared-shaped cell-laden collagen films resulted in a low tubular structure ratio. Our simulations in Figure 1B suggested a viable approach to control folding directions of flat, cell-laden collagen films to generate regular tubular structures by rendering mechanical anisotropy in collagen films. Such mechanical anisotropy could be achieved either through nonuniform patterning of cell distribution in collagen films or by introducing structural anisotropy in collagen films. In practice, it was difficult to achieve nonuniform patterning of cell distribution in collagen films in a controllable manner. Thus, in the present work, we integrated ridge array structures onto the backside of collagen films to introduce structural anisotropy in collagen films.

Simulation results showed that squared-shaped collagen films with ridge array structures would tend to fold along the direction perpendicular to the ridge array orientation (see Materials and Methods for details; Figure 3A). Theoretical calculations further confirmed that the moment of inertia (MI) for squared-shaped collagen films without ridge structures was homogeneous; however, for collagen films with ridge array structures, MI along the direction perpendicular to ridge array orientation (MI_x) was less than the value along ridges (MI_y) (Figure 3B). Thus, incorporating ridge array structures onto the backside of collagen films could effectively introduce mechanical anisotropy in collagen films.

Consistent with simulation and theoretical calculations, self-folding of square-shaped collagen films integrated with ridge structures indeed had a greater tendency to occur along the direction perpendicular to the ridge orientation (Figure 3C). Quantitative results confirmed that, with a TeloHAEC-GFP cell density of 2×10^6 cells mL^{-1}, tubular structure ratio increased from 0.28 ± 0.018 (flat without ridges) to 0.40 ± 0.029 (50 μm ridge) and 0.45 ± 0.030 (100 μm ridge) for a collagen concentration of 4 mg mL^{-1} and from 0.36 ± 0.012 (flat without ridges) to 0.74 ± 0.037 (50 μm ridge) and 0.80 ± 0.028 (100 μm ridge) for a collagen concentration of 6 mg mL^{-1} (Figure 3D). The folded structure ratio did not significantly change when comparing flat collagen films without ridges with those integrated with ridge structures (Figure 3D). This observation was consistent with the fact that self-folding of cell-laden collagen films was driven by cellular contraction. Thus, as integrated ridge array structures would not affect overall cellular contraction, the folded structure ratio should not change between flat collagen films without ridges and those integrated with ridge array structures.

We further confirmed the effect of ridge structures on improving tubular structure formation from self-folding collagen films using two additional cell lines (human umbilical vein endothelial cells, or HUVECs, and human normal lung fibroblasts). Specifically, for HUVECs, tubular structure ratio increased from 0.28 ± 0.005 (flat without ridges) to 0.38 ± 0.014 (50 μm ridge) and 0.52 ± 0.013 (100 μm ridge) with a gel concentration of 4 mg mL^{-1} and from 0.24 ± 0.049 (flat without ridges) to 0.70 ± 0.064 (50 μm ridge) and 0.75 ± 0.048 (100 μm ridge) with a gel concentration of 6 mg mL^{-1} (Figure 3D). For lung fibroblasts, tubular structure ratio increased from 0.23 ± 0.027 (flat without ridges) to 0.33 ± 0.019 (50 μm ridge) and 0.51 ± 0.073 (100 μm ridge) with a

DOI: 10.1021/acsbiomaterials.6b00468
ACS Biomater. Sci. Eng. XXXX, XXX, XXX−XXX

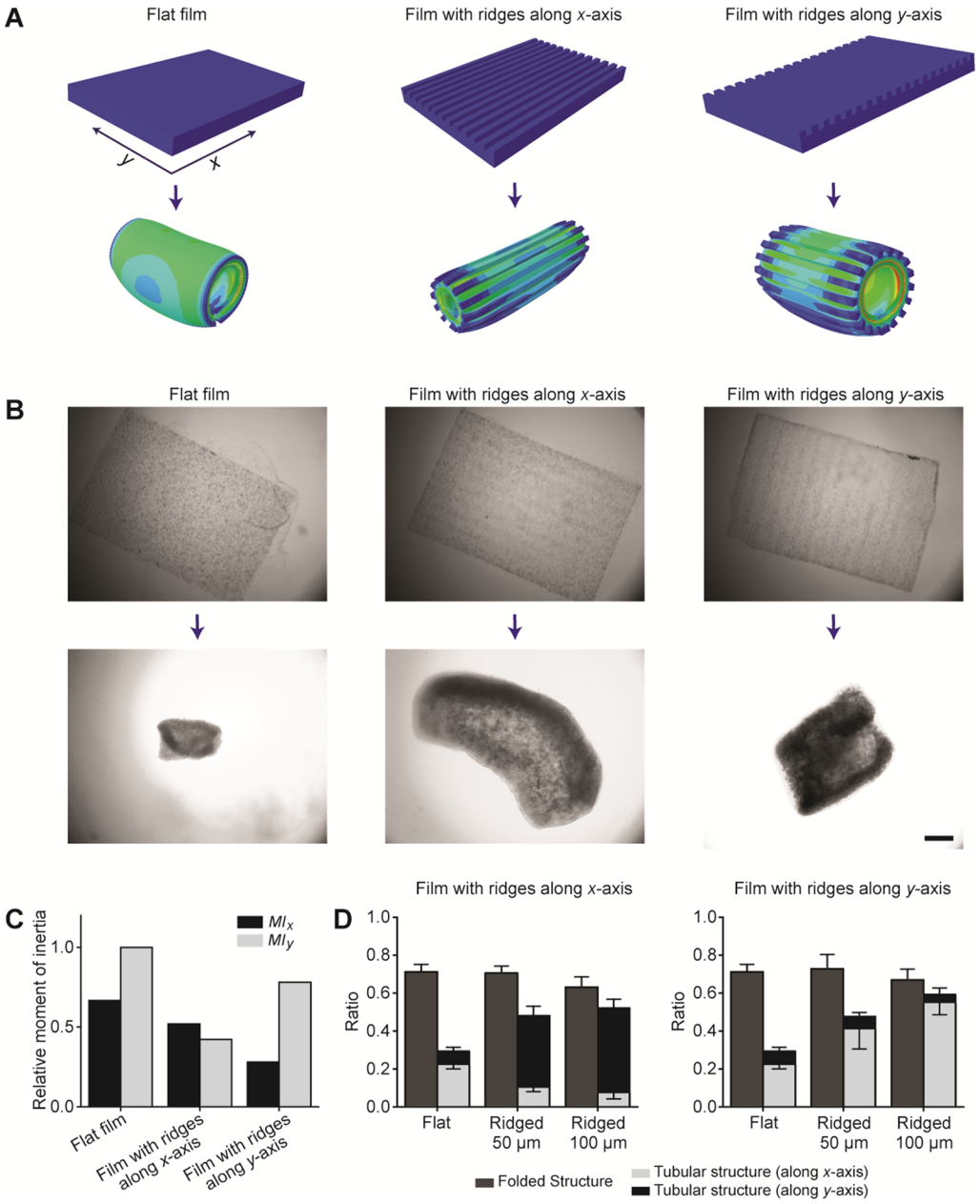

Figure 4. Ridge array structures integrated onto rectangular-shaped collagen films to facilitate collagen film folding. (A) Simulations showing folding of rectangular collagen films with a size of 2 mm × 3 mm integrated with 50 μm ridge array structures. The ridge array was arranged either along the long side (x-axis; middle) or along the short side (y-axis; right) of the collagen film. In simulations, collagen films were modeled as three-layered structures. The bottom layer had a thickness of 50 μm and an isotropic thermal expansion coefficient of 5 K^{-1}. The middle layer and the top ridge array had a thickness of 100 and 50 μm, respectively, and both layers had a homogeneous thermal expansion coefficient of 0 K^{-1}. For the 50 μm ridge array, ridge width and space were both 50 μm. All three layers in the collagen film had a Young's modulus of 20 KPa. In simulations, film temperature was set to decrease from −273.15 K (0 °C) to −293.15 K (−20 °C). (B) Representative bright field images showing collagen film folding with or without ridge structures as indicated. Top row showed flat collagen films at day 0, and bottom row showed folded collagen film structures at day 3. Scale bar, 500 μm. (C) Normalized theoretical moment of inertia (MI) values for collagen films with or without ridge array structures along the x- and y-axis as indicated. Data was normalized to the value for a flat collagen film along the y-axis. Please note that moment of inertial values for collagen films with 50 and 100 μm ridge arrays were the same. (D) Bar plots showing the effect of ridge structures on collagen film folding. A collagen concentration of 4 mg mL^{-1} was initially seeded with TeloHAEC-GFP cells with a cell density of 2 × 10^6 cells mL^{-1}. Error bars, s.e.m. with n = 3.

gel concentration of 4 mg mL^{-1} and from 0.31 ± 0.028 (flat without ridges) to 0.59 ± 0.018 (50 μm ridge) and 0.62 ± 0.022 (100 μm ridge) with gel concentration of 6 mg mL^{-1} (Figure 3D).

Ridge Structures Can Dominate Intrinsic Folding Tendency of Collagen Films. To further examine the effect of ridge array structures on controlling self-folding directions of collage films, we fabricated rectangular collagen films with a dimension of 2 mm × 3 mm. In simulations, such rectangular collagen films without ridge structures would naturally tend to fold along the long side of collagen films (x-axis in Figure 4A) as $MI_x < MI_y$ (see Materials and Methods for details; Figure

DOI: 10.1021/acsbiomaterials.6b00468
ACS Biomater. Sci. Eng. XXXX, XXX, XXX−XXX

4A−C). Simulations also showed that collagen films of 2 mm × 3 mm in size and integrated with ridge arrays would prefer to fold along the direction perpendicular to the ridge orientation, regardless of whether the ridge array was along the long or short side of collagen films (Figure 4A). Theoretical calculations of the moment of inertia further revealed that the difference between MI_x and MI_y became greater with the ridge array integrated along the *y*-axis of collagen films when compared to flat collagen films without ridge structures (Figure 4C). Importantly, relative magnitudes of MI_x and MI_y switched when the ridge array was oriented along the *x*-axis when compared to flat collagen films without ridge structures (Figure 4C), consistent with simulation results.

To confirm simulation and theoretical calculations, we conducted experiments to examine self-folding of rectangular collagen films with a dimension of 2 mm × 3 mm and a collagen concentration of 4 mg mL^{-1} seeded with TeloHAEC-GFP cells of a cell density of 2×10^6 cells mL^{-1} (Figure 4B). In experiments, folding directional preferences of 2 mm × 3 mm collagen films with or without ridge structures were consistent with simulation and theoretical results (Figure 4B). Quantitative results further confirmed that the ridge array structure not only increased significantly the tubular structure ratio but also dictated collagen film folding directions. Specifically, with the ridge array oriented along the *x*-axis, tubular structure ratio increased from 0.29 ± 0.023 (flat without ridges) to 0.48 ± 0.037 (50 μm ridge) and 0.52 ± 0.041 (100 μm ridge), among which tubular structures folded along the *y*-axis increased from 0.07 ± 0.012 (flat without ridges) to 0.38 ± 0.029 (50 μm ridge) and 0.44 ± 0.041 (100 μm ridge) (Figure 4C). When the ridge array was along the *y*-axis, tubular structure ratio increased from 0.29 ± 0.023 (flat without ridges) to 0.47 ± 0.065 (50 μm ridge) and 0.56 ± 0.017 (100 μm ridge), among which tubular structures folded along the *x*-axis increased from 0.22 ± 0.014 (flat without ridges) to 0.41 ± 0.062 (50 μm ridge) and 0.52 ± 0.035 (100 μm ridge) (Figure 4C).

CONCLUSION

Fabrication of microscale tubular structures in tissue engineering provides the promising opportunity for repairing and restoring functional loss of *in vivo* tissues such as blood and lymph vessels. Modular tissue engineering, given its advantage for recapitulating intricate tissue specific microenvironment and spatial cellular organization mimicking *in vivo* tissues, holds great promise for creating functional biomimetic 3D tissue constructs including tubular structures. In this study, we presented a simple yet robust microscale tissue engineering approach to generate tubular tissue units through cellular contractile force induced self-folding of cell-laden collagen films in a controllable fashion. Self-folding of cell-laden collagen films was driven by film contraction resulted from intrinsic contractile property of adherent mammalian cells seeded in collagen films. Through carefully designed experiments, we showed that both collagen gel concentration and cell density had significant impacts on self-folding of cell-laden collagen films. We further demonstrated using both experiments and theoretical modeling that folding directions of cell-laden collagen films could be controlled and tubular structure ratio could be significantly increased by adding ridge structures to the backside of collagen films to introduce structural anisotropy to collage films. One of the potential issues for the tubular structures generated by the method reported in this work was that the tubular structures were open-ended with bending film edges not merging together. Since in this current work collagen hydrogel was manually loaded into the PDMS mold, the size of the collagen film could not be too small. For future effort to scale up the fabrication of such tubular structures for modular tissue engineering applications, an automatic hydrogel loading system will be needed. Nevertheless, our approach of using ridge array structures to introduce mechanical anisotropy and thus promote tubular tissue unit formation can be extended to other biomaterial systems and thus provide a simple yet effective way to prepare tubular tissue units for modular tissue engineering applications.

ASSOCIATED CONTENT

Supporting Information

The Supporting Information is available free of charge on the ACS Publications website at DOI: 10.1021/acsbiomaterials.6b00468.

Schematic fabrication process of the PDMS mold and the initial cell distribution information (PDF)

AUTHOR INFORMATION

Corresponding Author

*E-mail: jpfu@umich.edu.

Notes

The authors declare no competing financial interest.

ACKNOWLEDGMENTS

We acknowledge financial support from the National Science Foundation (ECCS 1231826, CBET 1263889, and CMMI 1536087), the National Institutes of Health (R01 HL119542), the UM-SJTU Collaboration on Biomedical Technologies, the Michigan Center for Integrative Research in Critical Care (M-CIRCC), and the Michigan Translational Research and Commercialization for Life Sciences Program (MTRAC). The Lurie Nanofabrication Facility at the University of Michigan, a member of the National Nanotechnology Infrastructure Network (NNIN) funded by the National Science Foundation, is acknowledged for support in microfabrication.

REFERENCES

(1) Langer, R.; Vacanti, J. P. Tissue engineering. *Science* **1993**, *260* (5110), 920−6.
(2) Langer, R.; Vacanti, J. Advances in tissue engineering. *J. Pediatr Surg* **2016**, *51* (1), 8−12.
(3) Boublik, J.; et al. Mechanical properties and remodeling of hybrid cardiac constructs made from heart cells, fibrin, and biodegradable, elastomeric knitted fabric. *Tissue Eng.* **2005**, *11* (7−8), 1122−32.
(4) Tranquillo, R. T. The tissue-engineered small-diameter artery. *Ann. N. Y. Acad. Sci.* **2002**, *961*, 251−4.
(5) Correia, C. R.; et al. Chitosan scaffolds containing hyaluronic acid for cartilage tissue engineering. *Tissue Eng., Part C* **2011**, *17* (7), 717−30.
(6) Park, S. H.; et al. Development of dual scale scaffolds via direct polymer melt deposition and electrospinning for applications in tissue regeneration. *Acta Biomater.* **2008**, *4* (5), 1198−207.
(7) Silva, N. A.; et al. Development and characterization of a novel hybrid tissue engineering-based scaffold for spinal cord injury repair. *Tissue Eng., Part A* **2010**, *16* (1), 45−54.
(8) Thadavirul, N.; Pavasant, P.; Supaphol, P. Development of polycaprolactone porous scaffolds by combining solvent casting, particulate leaching, and polymer leaching techniques for bone tissue engineering. *J. Biomed. Mater. Res., Part A* **2014**, *102* (10), 3379−92.

DOI: 10.1021/acsbiomaterials.6b00468
ACS Biomater. Sci. Eng. XXXX, XXX, XXX−XXX

(9) Brown, D. A.; et al. Analysis of oxygen transport in a diffusion-limited model of engineered heart tissue. *Biotechnol. Bioeng.* **2007**, *97* (4), 962−75.
(10) Gauvin, R.; Khademhosseini, A. Microscale technologies and modular approaches for tissue engineering: moving toward the fabrication of complex functional structures. *ACS Nano* **2011**, *5* (6), 4258−64.
(11) Nichol, J. W.; Khademhosseini, A. Modular Tissue Engineering: Engineering Biological Tissues from the Bottom Up. *Soft Matter* **2009**, *5* (7), 1312−1319.
(12) Mironov, V.; et al. Organ printing: Tissue spheroids as building blocks. *Biomaterials* **2009**, *30* (12), 2164−2174.
(13) Fernandez, J. G.; Khademhosseini, A. Micro-masonry: construction of 3D structures by microscale self-assembly. *Adv. Mater.* **2010**, *22* (23), 2538−41.
(14) Yang, J.; et al. Tissue Engineering Using Laminar Cellular Assemblies. *Adv. Mater.* **2009**, *21* (32−33), 3404−3409.
(15) Torres-Rendon, J. G.; et al. Cellulose Nanofibril Hydrogel Tubes as Sacrificial Templates for Freestanding Tubular Cell Constructs. *Biomacromolecules* **2016**, *17*, 905.
(16) Baek, K.; et al. In situ self-folding assembly of a multi-walled hydrogel tube for uniaxial sustained molecular release. *Adv. Mater.* **2013**, *25* (39), 5568−73.
(17) L'Heureux, N.; et al. Human tissue-engineered blood vessels for adult arterial revascularization. *Nat. Med.* **2006**, *12* (3), 361−365.
(18) Walters, B. D.; Stegemann, J. P. Strategies for directing the structure and function of three-dimensional collagen biomaterials across length scales. *Acta Biomater.* **2014**, *10* (4), 1488−501.
(19) Moraes, C.; et al. Aqueous two-phase printing of cell-containing contractile collagen microgels. *Biomaterials* **2013**, *34* (37), 9623−31.
(20) Meghezi, S.; et al. Engineering 3D Cellularized Collagen Gels for Vascular Tissue Regeneration. *J. Visualized Exp.* **2015**, No. 100, e52812.
(21) Elamparithi, A.; Punnoose, A. M.; Kuruvilla, S. Electrospun type 1 collagen matrices preserving native ultrastructure using benign binary solvent for cardiac tissue engineering. *Artif. Cells, Nanomed., Biotechnol.* **2016**, 1−8.
(22) Alekseeva, T.; et al. Engineering a microvascular capillary bed in a tissue-like collagen construct. *Tissue Eng., Part A* **2014**, *20* (19−20), 2656−65.
(23) Rolfe, K. J.; Grobbelaar, A. O. A review of fetal scarless healing. *ISRN Dermatol* **2012**, *2012*, 698034.
(24) Ehrlich, H. P.; Hunt, T. K. Collagen Organization Critical Role in Wound Contraction. *Adv. Wound Care (New Rochelle)* **2012**, *1* (1), 3−9.
(25) Zhang, X.; et al. Flexible Fabrication of Shape-Controlled Collagen Building Blocks for Self-Assembly of 3D Microtissues. *Small* **2015**, *11* (30), 3666−75.
(26) Kuribayashi-Shigetomi, K.; Onoe, H.; Takeuchi, S. Cell origami: self-folding of three-dimensional cell-laden microstructures driven by cell traction force. *PLoS One* **2012**, *7* (12), e51085.
(27) Bowles, R. D.; et al. Self-assembly of aligned tissue-engineered annulus fibrosus and intervertebral disc composite via collagen gel contraction. *Tissue Eng., Part A* **2010**, *16* (4), 1339−48.
(28) Lopez-Garcia, M. D.; Beebe, D. J.; Crone, W. C. Young's modulus of collagen at slow displacement rates. *Biomed Mater. Eng.* **2010**, *20* (6), 361−369.
(29) Peterson, A. W.; et al. Vasculogenesis and Angiogenesis in Modular Collagen-Fibrin Microtissues. *Biomater. Sci.* **2014**, *2* (10), 1497−1508.
(30) Motte, S.; Kaufman, L. J. Strain stiffening in collagen I networks. *Biopolymers* **2013**, *99* (1), 35−46.

DOI: 10.1021/acsbiomaterials.6b00468
ACS Biomater. Sci. Eng. XXXX, XXX, XXX−XXX